In Situ Atomic Force Microscopy of Lithiation and Delithiation of Silicon Nanostructures for Lithium Ion Batteries

Collin R. Becker,[†,*] Kenneth E. Strawhecker,[‡] Quinn P. McAllister,[§] and Cynthia A. Lundgren[†]

[†]Sensors and Electron Devices Directorate, Energy and Power Division, U.S. Army Research Laboratory, ATTN: RDRL-SED-C, Adelphi, Maryland 20783, United States, [‡]Weapons & Materials Research Directorate, Materials and Manufacturing Sciences Division, U.S. Army Research Laboratory, ATTN: RDRL-WMM-G, Aberdeen Proving Ground, Maryland, 21005, United States, and [§]Weapons & Materials Research Directorate, Materials and Manufacturing Sciences Division, U.S. Army Research Laboratory, ATTN: RDRL-WMM-B, Aberdeen Proving Ground, Maryland 21005, United States. The manuscript was written through contributions of all authors. All authors have given approval to the final version of the manuscript.

ABSTRACT Using electron beam lithography, amorphous Si (a-Si) nanopillars were fabricated with a height of 100 nm and diameters of 100, 200, 300, 500, and 1000 nm. The nanopillars were electrochemically cycled in a 1 M lithium trifluoromethanesulfonate in propylene carbonate electrolyte. *In situ* atomic force microscopy (AFM) was used to qualitatively and quantitatively examine the morphology evolution of the nanopillars including volume and height changes *versus* voltage in real-time. In the first cycle, an obvious hysteresis of volume change *versus* voltage during lithiation and delithiation was measured. The pillars did not crack in the first cycle, but a permanent volume expansion was observed. During subsequent cycles the a-Si roughened and deformed from the initial geometry, and eventually pillars with diameters >200 nm fractured. Furthermore, a degradation of mechanical properties is suggested as the 100 and 200 nm pillars were mechanically eroded by the small contact forces under the AFM probe. *Ex situ* scanning electron microscopy (SEM) images, combined with analysis of the damage caused by *in situ* AFM imaging, demonstrate that during cycling, the silicon became porous and structurally unstable compared to as-fabricated pillars. This research highlights that even nanoscale a-Si suffers irreversible mechanical damage during cycling in organic electrolytes.

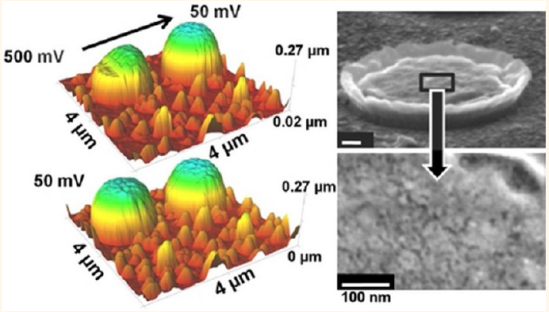

KEYWORDS: electron beam lithography · lithium ion batteries · atomic force microscopy · silicon · porous silicon

The continued rise of portable electronics and electric vehicles for personal, business, and military use drives an enormous demand for energy storage devices with massive energy density and unsurpassed efficiency, all without sacrificing safety. State-of-the-art Li ion batteries rely on graphite anodes and lithium-containing cathodes and offer impressive energy density and cycling stability.[1,2] However, unless new material systems are introduced, these batteries will not meet the demand for energy storage. For example, by replacing graphite anodes with silicon (Si) anodes, up to a 30% gain in capacity can be realized using currently available cathode materials.[3] Furthermore, more advanced cathode materials may someday make use of the extremely high energy capacity of Si compared to graphite (~3500 *vs.* 372 $mAhg^{-1}$).[4] However, while graphite stores Li by an intercalation process, Si stores Li using an alloying process.[5] A $Li_{4.4}Si$ alloy is formed at maximum lithiation that corresponds to over 300% volume expansion of the original Si material.[5,6] Upon repeated cycling, the Si electrode fractures and leaves Si fragments electrically isolated or debonded from the current collector, which leads to rapid capacity fade of the battery.[7] Additionally, as cracks open, new Si surfaces are exposed to electrolyte, and while Si is typically considered an inert material, it is actually extremely reactive in oxidizing environments.[8−11] Consequently, the freshly exposed Si is consumed as it reacts with the

* Address correspondence to collin.r.becker.civ@mail.mil.

Received for review July 22, 2013 and accepted August 31, 2013.

Published online August 31, 2013
10.1021/nn4037909

© 2013 American Chemical Society

electrolyte to generate solid electrolyte interphase (SEI).[12,13] Therefore, knowledge of the morphology *in situ* and mechanical stability evolution of nanoscale Si in conventional nonaqueous electrolytes is required to engineer Si anode−electrolyte combinations that are structurally stable and resist chemical attack of the Si anode by the electrolyte.

While nanoscale Si is generally known to resist fracture and accommodate the volume expansion and contraction during lithiation and delithiation better than bulk Si,[3,14] more work is required to understand the differences between crystalline Si (c-Si) and amorphous Si (a-Si) during electrochemical cycling. For example, it has been observed that while nanoscale c-Si avoids fracture when critical dimensions are below 150−300 nm, a-Si spheres do not fracture even when the diameter is as large as 870 nm.[15] The resistance to fracture may arise from faster bond breaking kinetics relative to diffusion of Li^+ in Li_xSi that leads to a larger concentration gradient and reduced stress relative to c-Si.[15] Additionally, c-Si is known to expand anisotropically, while a-Si expands isotropically, and the lithiation reaction velocity remains constant rather than slowing as in c-Si during lithiation.[15−17] Furthermore, self-limiting lithiation resulting from stress has been observed for c-Si wires and particles, and a c-Si core remains until the particle cracks and only then fully lithiates.[18,19] Finally, during lithiation on the first cycle, the c-Si becomes amorphous Li_xSi and forms crystalline $Li_{15}Si_4$ below about 60 mV, but even upon delithiation the Si remains amorphous.[20,21] Crystallization of a-Si to $Li_{15}Si_4$ in a-Si films coated on carbon nanofibers has also been observed,[22] but another study of a-Si nanospheres was inconclusive on the formation of crystalline $Li_{15}Si_4$.[15] Since the lithiation and delithiation of a-Si or a-Si composite materials proceed similarly to c-Si but with reduced fracture, more studies are necessary to reveal how best to incorporate a-Si into high capacity battery anodes.

Shape and morphology changes of nanoscale c-Si and a-Si during electrochemical cycling have been monitored *in situ* and *ex situ*.[15,16,18] Many of these studies have been motivated by initial work showing that nanometer sized anodes resist fracture relative to larger sized anodes.[3,14] Using *in situ* transmission electron microscopy (TEM), researchers have discovered interesting phenomena including self-limiting lithiation of c-Si and two phase lithiation of a-Si.[15,18,19] Additional *in situ* TEM studies have investigated Si/carbon, germanium (Ge), and tin oxide (SnO_2) nanowires and nanoparticles.[22−25] *In situ* TEM allows for extremely high resolution imaging including structural and chemical analysis with the trade-off that vacuum compatible electrolytes such as ionic liquids or solid state electrolytes, rather than conventional organic electrolytes, must be used.[25] Several studies using *ex situ* scanning electron microscopy (SEM) of Si nanostructures cycled in liquid organic electrolytes have found that fracture of c-Si is highly anisotropic and below a certain size, c-Si wires avoid cracking.[16,26] Additionally, atomic force microscopy (AFM) has been used *ex situ* to record the volume and height changes of micrometer sized a-Si pillars that resulted in severe cracking of the pillars after 5 cycles.[27]

A limited number of *in situ* AFM studies of Si have been published, and none have focused on submicrometer Si geometries.[5,28] *In situ* AFM is extremely valuable, as it offers both nanoscale resolution and the ability to study Si lithiation, Si delithiation, and SEI formation in a liquid, organic electrolyte. Also, the AFM can image a sample during numerous charge and discharge cycles all while collecting electrochemical data from a standard potentiostat. The objective in the present work was to use *in situ* AFM to both monitor morphology changes of nanoscale Si and use the AFM probe to physically interact with Si anodes to gain a qualitative understanding of the mechanical integrity of the structures. Here, nanoscale a-Si pillars were fabricated using electron beam lithography (EBL) so that anodes with precise geometry could be realized rather than relying on chemical synthesis or etching techniques that lead to a distribution of sizes. This allowed for a measurement of volume and height changes in real time and across a span of pillar diameters from 1000 to 100 nm. Lastly, by analyzing *ex situ* SEM images, comparisons were drawn between pillars that had been perturbed by the AFM probe during cycling and those that had not been imaged by the probe during cycling.

RESULTS AND DISCUSSION

Silicon nanopillars are fabricated in a multistep fabrication scheme using EBL and liftoff techniques, the details of which are given in the Methods section. The current collector for the pillars is a 400 nm thick nickel (Ni) film evaporated on a (100) Si wafer. A 100 nm thick layer of a-Si (Supporting Information, Figure S1) was deposited by electron beam evaporation to generate arrays of a-Si nanopillars with diameters of 100, 200, 300, 500, and 1000 nm and spaced 2 μm apart center-to-center. Figure 1a shows a schematic of the pillars, and Figure 1b shows an atomic force microscope (AFM) image of the as-fabricated pillars. In this paper, the pillars are referenced by the initial designed diameters, with the actual diameters as measured by SEM given in the Methods section. The AFM imaging was conducted while using the a-Si pillar chip as the working electrode in a custom electrochemical cell. The cell was filled with 1 M lithium trifluoromethanesulfonate ($LiCF_3SO_3$) in propylene carbonate electrolyte. A piece of Li metal (all voltages in this communication are referenced to the Li/Li^+ couple) served as the counter and reference electrode.

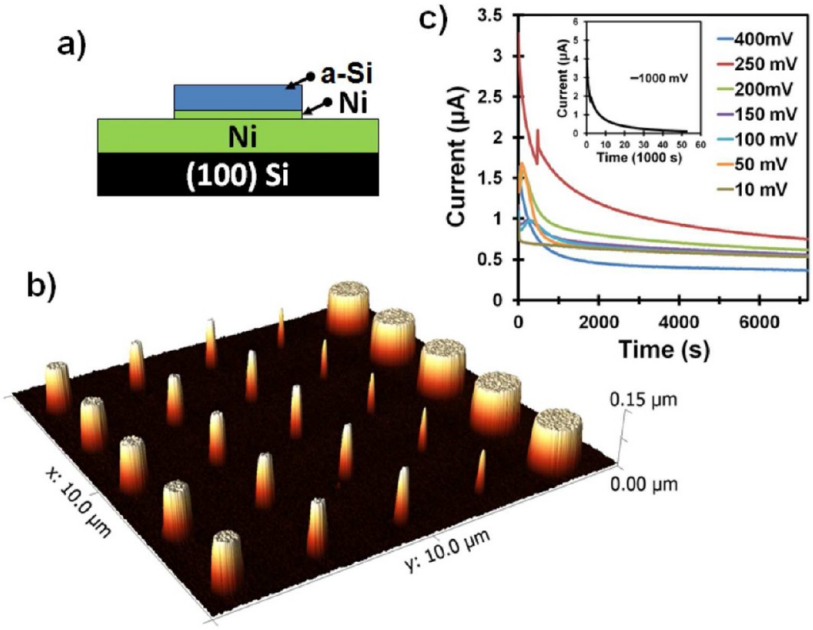

Figure 1. (a) Schematic of a-Si pillars on Ni substrate, (b) AFM image showing the as-fabricated array of 1000, 500, 300, 200, and 100 nm diameter pillars, and (c) current profiles of the various potential holds (the inset shows the 1 V hold) on the first cycle of the a-Si pillars on Ni substrate.

For electrochemical testing, potentiostatic methods were used to monitor the evolution of the a-Si at specific voltages that thermodynamically limited the amount of Li that was alloyed. The specific testing protocol is presented in the Methods section, but briefly, to gain an understanding of the nanopillar morphology evolution, potentiostatic holds at several voltages between open circuit potential (OCP) and 10 mV during lithiation and delithiation were chosen. Representative electrochemical data showing the current decay with time at each potential hold during lithiation is shown in Figure 1c. The sample was held for 2 h at each potential except for holding for 8 1/2 h at 10 mV while imaging a region of pillars to ensure the volume change of the pillars had ceased. For each voltage step, the current fell below 1 μA but never fully dissipated despite only having 1 μAh of capacity per die. No cracks in the Ni layer were observed using *in situ* AFM or *ex situ* SEM, indicating that the Ni served as an effective barrier against Li intercalation of the Si wafer. Therefore, the residual current could possibly be related to the trace contaminants in the electrolyte, underpotential deposition (UPD) of lithium, and/or reductive decomposition of PC on the Ni current collector.[28−30]

After the final hold at 10 mV, the sample was delithiated, and then it was cycled one additional time as described in the Methods section. AFM images of the a-Si pillar morphology evolution during the first cycle are shown in Figure 2. Growths from UPD of Li or reductively decomposed electrolyte, consistent with prior observation, were observed on the Ni substrate.[29,30] The growths on the substrate were first observed at ~350 mV and were robust in that they could not be removed by the AFM probe and only slightly shrank upon returning to 2 V. The a-Si nanopillars began to grow between 400 and 250 mV, and the pillars adopted a conical shape. Large growths like those on the Ni were never observed on top of the pillars during imaging. Upon delithiation, the pillars recovered a flat top and shrank in height.

In Figure 3a−c and Figure 3d−f, the volume expansion/contraction and the height expansion/contraction of the 1000, 500, and 200 nm diameter a-Si pillars, respectively, are plotted *versus* voltage for the first two cycles (values for the 300 and 100 nm pillars are reported in the Supporting Information, Figure S2). The error bars in Figure 3 represent the span of the data measured from three pillars of each size. The reported values are taken during a potentiostatic segment from 4708 to 7062 s into the hold at each potential. At 400 mV, only small amounts of volume and height change were observed. Then, at each step in voltage between 250 and 10 mV, a nearly linear increase in both height and volume was observed. On the first cycle the 1000−200 nm pillars achieved 288 ± 14%, 299 ± 27%, 362 ± 66%, and 265 ± 40% volume expansion, respectively, but the 100 nm pillars only attained 158 ± 17%. The maximum volume change of the pillars is expected to be about 320%, which agrees closely to measured volume changes with all sizes except the 100 nm pillars.[27] The percentage height increase for the pillars decreased with pillar diameter and was highest 159 ± 16% for the 1000 nm, and lowest 48 ± 20% for the 100 nm pillars. The dashed line in Figure 3a−c represents expected volume change

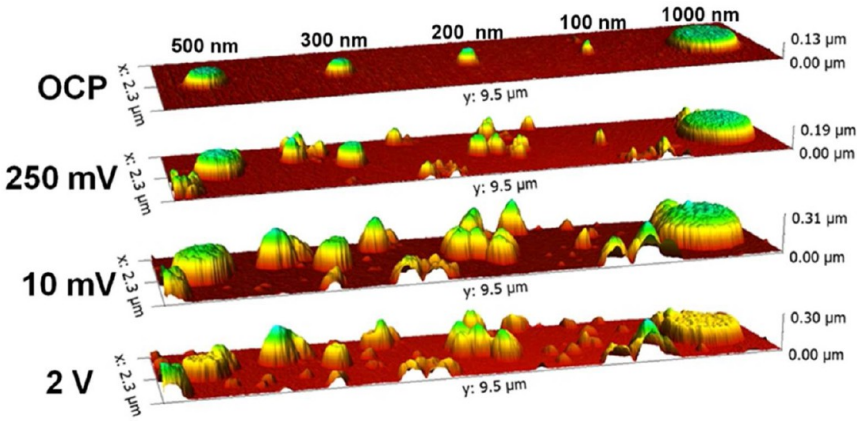

Figure 2. *In situ* **3D AFM images during lithiation and delithiation of a-Si nanopillars taken at several electrochemical potentials in the first cycle.**

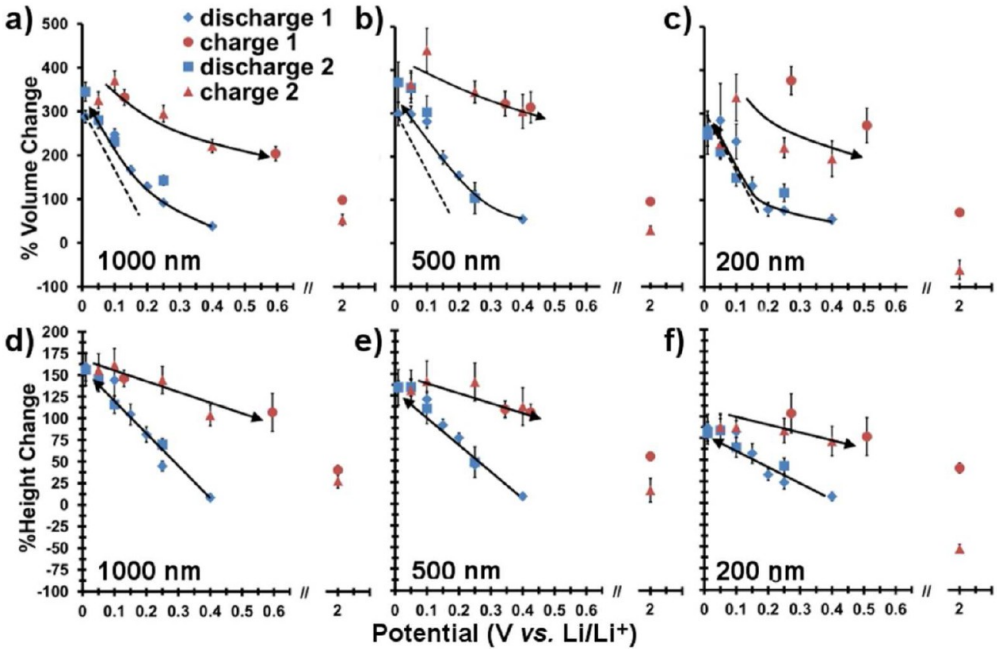

Figure 3. *In situ* **AFM measurements of % volume and % height change of a-Si nanopillars during the first two discharge (lithiation) and charge (delithiation) cycles as a function of potential. (a−c) % Volume change of the 1000, 500, and 200 nm pillars, respectively. (d−f) % Height change of the 1000, 500, and 200 nm pillars, respectively. The arrows in the figures are intended only to guide the eye and do not represent a mathematical fit to the data. The dashed lines in (a−c) represent expected volume change with potential.[27,31]**

versus potential.[27,31] The AFM measured volume changes for the 1000−300 nm pillars in Figure 3a,b and Supporting Information, Figure S2, lie considerably above this line until 50−100 mV, but the 200 nm pillar volume changes in Figure 3c lie extremely close to the predicted values. The 100 nm pillar volume changes (Supporting Information, Figure S2), are lower than predicted.

The volume change of the 200−1000 nm diameter pillars is consistent with prior studies on micrometer scale a-Si.[27,28] However, the volume change of the 100 nm pillars was considerably less than the larger pillars. Using *in situ* TEM, McDowell *et al.* observed that a-Si spheres as large as 870 nm in diameter experienced a volume increase that varied from 101 to 332% and did not fracture.[15] The authors reported that the variability in the measurements and observation of lower than expected volume change may have resulted from experimental conditions such as poor electrical contact to particles. They also state there is a possibility that in c-Si more Li is accommodated in the Li_xSi phase when Si−Si bonds are broken compared to breaking of Si−Si bonds in a-Si. In the current work, the electrical connection is expected to be quite robust as the pillars remain bonded to the Ni substrate. However, the lower than expected volume increase of the 100 nm pillars may result from the apparent weakening of the structure of the pillars during electrochemical

cycling and subsequent erosion by the AFM tip, which will be discussed later in this paper. The small size of the 100 nm pillars makes the measurement of volume change especially sensitive to even minor erosion by the AFM tip.

The measured height change of the pillars in the current work is significantly lower than that measured *in situ* by Beaulieu *et al.* (~275%) but similar to that measured *ex situ* by He *et al.* (160−180%).[27,28] Those studies used films of 300−500 nm thickness and patterned features with lateral dimensions of 5 μm × 5 μm or 7.6 μm × 7.6 μm. The cause of these discrepancies in height change may be a result of the quality of adhesion of Si to the current collector. Beaulieu *et al.* studied Si on a copper current collector and reported negligible lateral dimension change, whereas He *et al.* used a titanium current collector and reported expansion of ~35% in width and an evolution of the pillar to a circular shape from a square shape. Here, using a Ni current collector the pillars are circular initially, and a diameter increase is observed during cycling that is able to recover after the first cycle, as will be discussed later. Size scale, geometry, and adhesion to the current collector all likely affect the pillar morphology evolution, and further work is required to fully understand the differences in the studies.

Lastly, the ratio of the % height growth to the % volume growth (expansion ratio) is shown in Figure 4. The volume change is proportional to the height change; therefore, the closer the expansion ratio is to 1:1, the less the pillar diameter is expanding. The largest expansion ratios are for the 1000 and 500 nm pillars, suggesting the larger pillars expand more in height (relative to the smaller pillars) while the smaller pillars expand more in diameter (relative to the larger pillars). Additionally, *ex situ* SEM images in Figure 5a−f from a separate sample that has been rinsed with water to etch any remaining SEI or remaining Li show that after one cycle, the pillars now have slightly more vertical sidewalls. Other than slightly more vertical sidewalls they appear almost unchanged from the as-fabricated samples, and the diameters as measured by SEM have returned to the initial values. This is in contrast to a prior study of micrometer scale a-Si pillars, which saw permanent deformation after one cycle, and to studies on nanoscale c-Si that exhibited fracture when the pillars assumed full volume expansion.[19,27,32]

Upon charging (delithiation), a large overpotential, observed as a hysteresis in Figure 3 both in height and volume, was required to initiate volume and height contraction. We note this hysteresis was observed on both the first cycle where the pillars simply ramped back to 2 V and on the second charge when allowing 2 h of equilibration at several potential steps. This overpotential has been correlated to stress-potential coupling and plastic

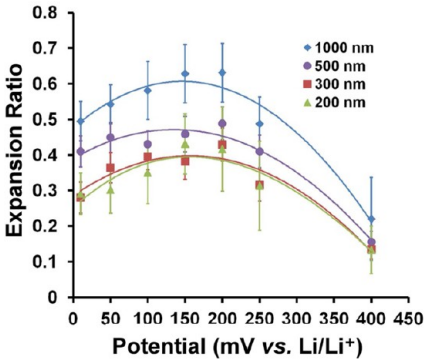

Figure 4. Plot of the ratio of % height change to % volume change (expansion ratio) of the 1000−200 nm pillars as measured by *in situ* AFM imaging. The lines in the figures are intended only to guide the eye and do not represent a mathematical fit to the data.

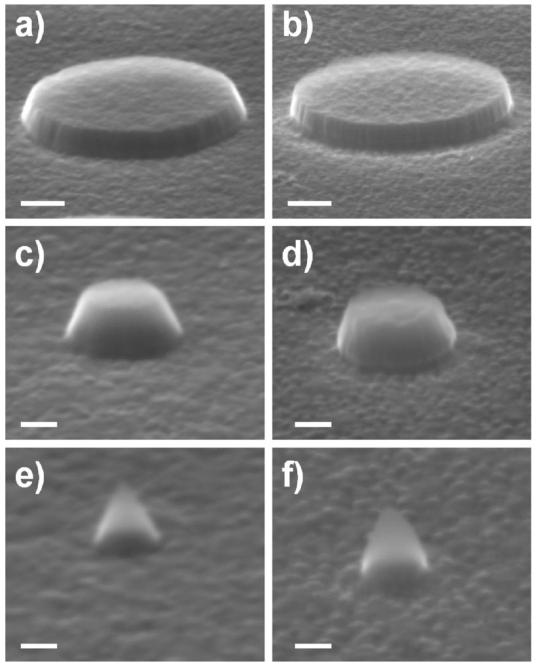

Figure 5. *Ex situ* SEM images of 1000 nm (a,b); 300 nm (c,d); and 100 nm (e,f) a-Si nanopillars, as fabricated (a,c,e) and after 1 cycle, (b,d,f). Scale bars are 200 nm in (a,b) and 100 nm in (c−f).

deformation.[33,34] Also, after returning to 2 V on the first cycle, the volume increases from the initial volumes were 98 ± 5%, 96 ± 5%, 88 ± 5%, 72 ± 7%, and 86 ± 7% for the 1000−100 nm pillars, respectively. The inability of a-Si nanoparticles to return to the initial volume has also been observed by *in situ* TEM.[15] Since the images in Figure 5a−f in which SEI has been etched show the pillars are nearly unaffected by one electrochemical cycle, the measured volume increase by AFM may be a combination of the buildup of SEI, decrease in density and likely porosification of the a-Si upon delithiation, and incomplete delithiation. Also, the now more vertical sidewalls may add to slight overestimation of volume by the AFM tip. Although the pillars suffered a permanent expansion, they did regain

a shape nearly the same as the initial shape after one cycle, which differs from the bowl shape adopted by micrometer scale features studied in prior work by He *et al.*[27] Additionally, the second discharge (lithiation) followed the first lithiation very closely, but the final volume increase was slightly higher in the 1000 and 500 nm pillars at 345 ± 22% and 372 ± 47%, respectively. The nanopillars in the current work are circular as opposed to the square pillars studied by He *et al.*, so the lack of sharp corners that may concentrate stress likely plays a role in the ability of the features here to recover after the first cycle.

Since AFM and SEM images revealed that the pillars could accommodate the volume change on the first cycle without fracturing, an additional test on a separate sample cycled pillars for 5 times. The SEM images (Supporting Information, Figure S3) taken after rinsing with water to etch SEI reveal that the pillars have now plastically deformed and roughened. The ability of the pillars to recover in morphology after one cycle is interesting given that Si typically displays a very poor first cycle efficiency and indicates mechanical instability, degradation, or adhesion to the current collector is not the only cause of this loss.[3] The next 5 cycles though clearly begin to degrade the pillar, and plastic deformation is occurring.

Since fracture or cracking was not observed even after 5 cycles, as opposed to prior studies of thin film structures,[27] we subjected the pillars from the AFM test to 25 additional cycles at a fast rate of 2.5 mV/s without any potentiostatic holds. The pillars were then removed from the AFM cell, rinsed with water to etch away any SEI or Li present in the sample, and imaged by SEM. It is emphasized that for these 25 cycles, the AFM position was moved to a region of pillars that had yet to be imaged, and only then the AFM began imaging (*i.e.*, the AFM probe came into physical contact with the pillars during the next 25 cycles). The SEM images clearly revealed the region where the AFM had imaged as an area relatively free of deposits, so micrographs of both imaged and nonimaged pillars were readily taken. Images of as-fabricated 1000 and 200 nm pillars are shown in Figure 6a,b, respectively. The 1000 and 200 nm pillars that were rinsed with water after cycling are shown in Figure 6c–h. The pillars shown in Figure 6c (1000 nm) and Figure 6d (200 nm) were not imaged by the AFM during cycling. The 1000 nm pillar in Figure 6c has an outer ring of material that cracked from the main body. The ring of material was not etched by the water rinse and is therefore likely not a buildup of SEI material or UDP Li. In contrast the 200 nm pillar in Figure 6d is somewhat deformed in shape but generally remained intact. Figure 6e (1000 nm) and Figure 6f (200 nm) are magnified images of the top surface of the pillars. While the etched 1000 nm pillar was highly porous (see Figure 6e), the etched 200 nm pillar did not exhibit visible porosity

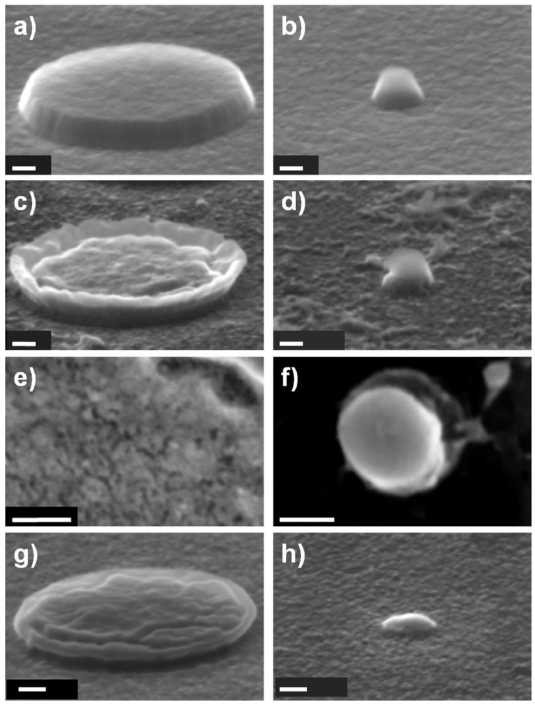

Figure 6. *Ex situ* SEM images of a 1000 nm (a,c,e,g) and 200 nm nanopillar (b,d,f,h). (a,b) as fabricated; (c,d) after 2 slow electrochemical cycles followed by 25 fast electrochemical cycles without concurrent imaging by the AFM; (e,f) top-view and magnified image of (c,d), respectively; and (g,h) pillars that were subjected to the same electrochemistry as (c,d) but were imaged with the AFM during cycling. Scale bars are 100 nm.

(see Figure 6f). In prior work, the Si structure remained stable until the 20th cycle, at which point it adopted a wrinkled structure, as observed by *ex situ* TEM.[4] This is similar to the current work, where for a low number of cycles, the pillars remained reasonably unchanged, and then after 25 cycles, nanopores and "macro" scale cracks were observed. It should also be noted that pillars remained attached to the current collector even after 25 fast cycles, indicating that the Ni–Si interface is very robust, and a loss of Si material from the body of the pillar rather than delamination from the current collector would lead to a loss of capacity.

Pillars that were continually imaged by AFM during cycling are shown in Figures 6g (1000 nm pillar) and Figure 6h (200 nm pillar). The 1000 nm pillar that was continually imaged by the AFM also had a ring structure, but the ring was thinner compared to the nonimaged sample, suggesting possible erosion of the outer ring due to interaction with the AFM tip. The imaged 200 nm pillar (Figure 6h) appeared to have been completely eroded by the AFM tip. Finally, several pillars were scanned by the AFM probe only once, and only *after* electrochemical cycling was complete but while the sample was still submerged in electrolyte. SEM images of these pillars show that the 1000, 500, and 300 nm pillars were severely damaged by the single scan (*i.e.*, pillar cracking was more significant for

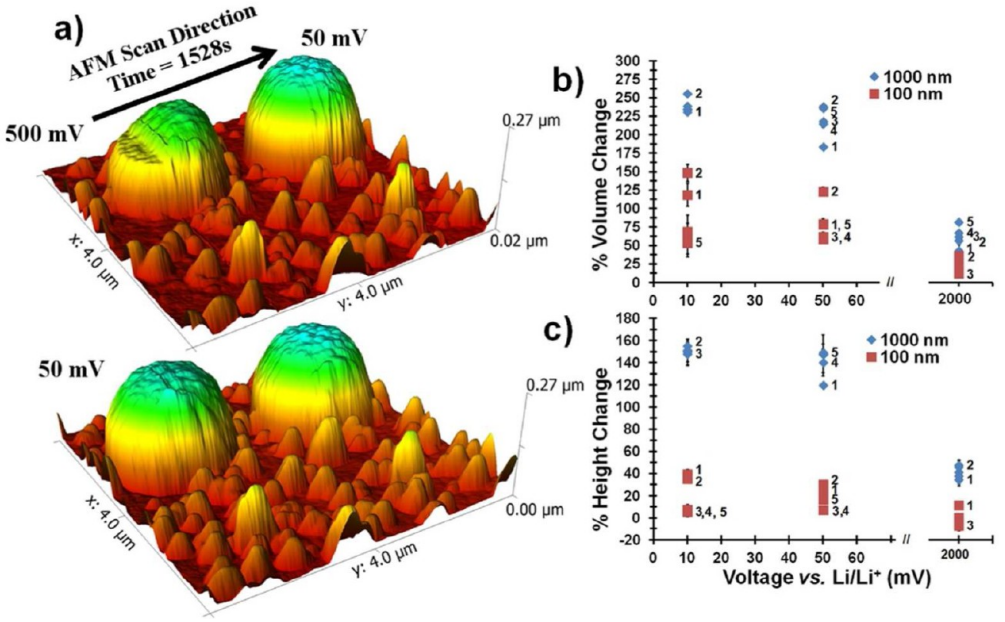

Figure 7. (a) *In situ* AFM image showing the growth of the 1000 and 100 nm a-Si nanopillars during AFM scanning and electrochemical cycling at 1 mV/s. (b,c) Volume and height percentage change for each of the 5 cycles at 1 mV/s. The number labels correspond to the cycle at which each measurement was made. Labels are omitted for clarity where values overlap.

the pillars that had been touched by the AFM probe than pillars that had not been touched, Supporting Information, Figure S4). The 200 and 100 nm pillars remained intact, but the 100 nm pillar was eroded by the single AFM scan (Supporting Information, Figures S5c and S6c, 100 and 200 nm, respectively). Therefore, the Si structure remaining after cycling may be highly porous and fragile enough to be damaged even by the light contact forces under the AFM probe. It is important to note that such pillar degradation during cycling is not readily observed when using noncontact microscopy-based imaging techniques.

The charge–discharge rate may also significantly affect the morphological evolution of a-Si nanopillars during lithiation. The effect of the charge–discharge rate on the pillar morphology was studied on a separate sample that was cycled 5 times at 1 mV/s (rather than 0.25 mV/s) between 2 V and 10 mV for 5 cycles, with potentiostatic holds of 2 h each only at 50 mV, 10 mV, and 2 V. This test procedure results in a relatively instantaneous discharge to 50 mV compared to our first test protocol of stopping at numerous potentials for 2 h each. The test is thus designed to determine if a rapid lithiation rate will cause plastic deformation or fracture in the first few cycles. As captured in real-time on the second cycle, volume expansion initiates at 167 mV (see Figure 7a), which is nearly 100 mV lower than the pillars cycled at the slower rate with more voltage holds. The significance of this requires further investigation, but the real-time imaging of silicon lithiation with AFM is demonstrated by this technique. Since the small undulations can be resolved in the pillar by AFM and the image is extremely clear, any SEI that forms can be presumed to be quite uniform and is reasonably hard such that it does not interfere with imaging. The volume and height changes of the largest (1000 nm) and smallest (100 nm) pillars studied herein at each of the potential holds for 5 cycles are shown in Figure 7b,c. The maximum volume expansion of the pillars that were ramped at 1 mV/s occurred on the order of only a few hundred seconds (based on the 1 mV/s rate), and the 1000 nm pillars limited expansion to 231–256%. The 100 nm pillars, within experimental variation, demonstrated a nearly identical volume increase as in the initial slow cycling test. Both sizes of pillars, within experimental variation, grew to the same height as the initial test. The volume and height change was smallest during the first cycle for the 1000 nm pillar but largest during the first cycle for the 100 nm pillar. By the fifth cycle, the 100 nm pillar exhibited nearly zero height change and only about 30–50% volume change. No fracture or large cracks were observed by the AFM in either size of pillar. The volume limit in the 100 nm pillar again is likely related to erosion of the pillar, especially since the height change was negligible after 5 cycles. The fact that the 1000 nm pillar limited volume expansion indicates that at a faster rate, lithiation may proceed differently or to a lesser extent than when the pillar is allowed to equilibrate at several potentials and is cycled slowly.

As a final investigation, the difference observed in the degradation of the smaller 100 and 200 nm pillars (erosion) and the larger 300, 500, and 1000 nm pillars (cracking) may be related to the extent of lithiation of the pillar bulk. To qualitatively identify the extent of lithiation in the pillar bulk, we fully lithiated a separate sample of pillars by holding the sample at a 10 mV

potential after 7 initial cycles until any structural changes observed by AFM during cycling had ceased. The sample was then removed from the cell, rinsed with DEC, transferred to an SEM, and imaged with only minimal exposure to laboratory air. Next, the Li and any SEI were etched from the a-Si nanopillar by immersing the pillars in water. SEM images prior to water rinsing of the 1000, 300, and 200 nm pillars that had been imaged by the AFM while being lithiated at 10 mV are shown in Figure 8a,c. Finally, the pillars after the water rinse (these pillars had not been imaged by the AFM) are shown in Figure 8b,d,e. The 1000 and 300 nm pillars assumed a bowl shape after etching with water. On the other hand, the 200 nm pillars, Figure 8d, did not have a crater in the middle. The remaining "core" of the smaller pillars must be Li-free, since the water rinse etches any SEI or Li containing materials. Furthermore, any SEI that formed on the a-Si must be relatively thin, as the images in Figure 8a,c do not show a dramatic difference relative to Figure 8b,d other than in actual removal of pillar material and cleanliness of the Ni surface. This corroborates the AFM data where the volume change of the pillars was on the order of that expected for full Si lithiation that suggests the pillars lacked any sort of thick, soft SEI layer.

The pillar structure that remained after water etching provides insight on the lithiation process of the pillars. The outer regions of the smaller pillars (100 and 200 nm) were completely etched and therefore likely completely lithiated; however, the core of the pillars remained, suggesting that the pillars are not fully lithiated in the center. On the contrary, the larger pillars leave a nonlithiated region at the outer edge of the pillar, which is likely related to the ring of material that cracked away from the core of the pillars and is shown in Figure 6c.

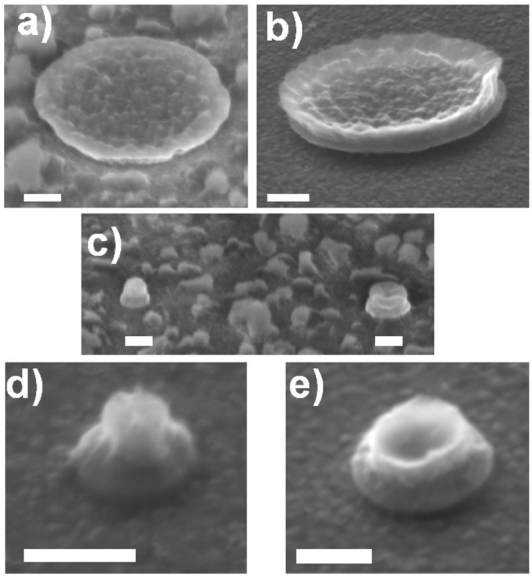

Figure 8. (a–e) *Ex situ* SEM images of Si nanopillars. (a) The 1000 nm pillar after removing from the electrochemical cell while held at 10 mV. (b) The same pillar as (a) but rinsed with water to etch SEI and Li from the sample. (c) The 200 nm (left) and 300 nm (right) pillars, respectively, in the same condition as (a). (d,e) The 200 and 300 nm pillars, respectively, after rinsing with water, as in (b). All scale bars are 200 nm.

CONCLUSION

In situ AFM and *ex situ* SEM were used to analyze nanometer sized a-Si pillars 100 nm tall and 100–1000 nm in diameter during lithiation and delithiation. The AFM was used to directly observe the nanoscale shape evolution of the pillars during cycling. The pillars with diameters of 200 nm or larger reached the theoretical volume expansion of ~300%. The volume expansion of the 100 nm pillars was limited however to below 200%. All of the pillars were roughened during cycling but were not cracked after 5 cycles as micrometer sized Si anodes have demonstrated in other studies. However, after 27 cycles, pillars 300 nm in diameter and larger did crack, while the 200 and 100 nm pillars remained intact. When the nanopillars were subjected to AFM imaging during or after cycling, the pillars of all sizes were clearly damaged or eroded. Thus, the a-Si nanopillars were fragile enough after cycling to be damaged under the light contact forces with the AFM tip due, at least in part, to the formation of a porous structure observed with SEM. Imaging with AFM and preferential etching of Li containing regions from fully lithiated pillars also showed that the 100 and 200 nm pillars grew in a more isotropic fashion than larger pillars, which tended to grow more upward than outward. Consequently, when fully lithiated pillars are etched by water, the 100 and 200 nm pillars had only a small core remaining, while the larger pillars possessed a ring of material on the outer boundary of the pillar.

In terms of practical cyclability of Si anodes, the current work demonstrated that a-Si nanopillar anodes ranging in diameter from 100 to 1000 nm were mechanically damaged during electrochemical cycling. The damage mechanisms were pillar size-dependent. Larger a-Si pillars cracked, while smaller a-Si pillars were weakened, despite appearing to be intact. The a-Si material is apparently unable to regain its initial mechanical properties upon delithiation and, over several cycles, simply begins to break down. Without additional engineering to protect the anode, even nanoscale a-Si material is not mechanically robust during cycling. While many groups have seen capacity fade in Si anodes, the present work specifically measures the dimensions and gains a qualitative understanding of the actual a-Si structures as they degrade during cycling. Therefore, it is imperative to understand the *in situ* changes in the material properties of the anodes during cycling that likely have significant implications on the cyclability of a real battery. This qualitative observation of the decreased structural

integrity of the pillars motivates future research on the *in situ* quantification of Si nanopillar mechanical properties that will guide both theoretical and experimental studies.

METHODS

Nanopillar Fabrication. The amorphous silicon (a-Si) nanopillars were fabricated on a substrate consisting of a 400 nm thick layer of nickel (Ni) on a (100) Si wafer. The Ni layer was electron beam evaporated onto the Si wafer using an Evatec BAK 641. After depositing the Ni, the substrate was patterned by electron beam lithography (Vistec EBPG5000+ES) using a bilayer poly(methyl methacrylate) (PMMA) photoresist. A 20 nm Ni adhesion layer followed by a 100 nm thick layer of a-Si (or Ni for the Ni pillar arrays) were then deposited (also by electron beam evaporation) onto the patterned wafer forming ~100 nm tall a-Si nanopillars. The Si wafer was then diced into ~1.5 × 1.5 cm chips containing 100 grids of 100 × 100 pillars chips to be used for AFM testing. As measured by SEM from the base of the pillars, the 1000−100 nm pillars measured 1033 ± 4 nm, 530 ± 10 nm, 329 ± 5 nm, 226 ± 1.5 nm, and 124 ± 2 nm, respectively.

Electrochemical Testing. To limit exposure to moisture, all testing was conducted in a dry room with a dew point of less than −80 °C. The sample was cycled from open circuit potential (OCP) to 1 V at a rate of 0.25 mV/s. The sample was then held at 1 V overnight to allow contaminates, such as water in the electrolyte, to decompose, which helped reduce the background current at subsequent potential holds. The sample was then lithiated by decreasing the voltage at a rate of 0.25 mV/s. During the voltage ramp down, holds were performed for 2 h each at 400, 250, 200, 150, 100, 50 mV and for ~8 1/2 h at 10 mV. The sample was delithiated by allowing the cell to relax for 10 min under open circuit conditions to 200 mV. Upon reaching 200 mV, the voltage was ramped to 2 V at a rate of 0.25 mV/s. The sample was then discharged (lithiated) for a second cycle in the same manner as the first cycle. During the subsequent charge (delithiation) in the second cycle, the sample was also held at 50, 100, 250, 400 mV and 2 V. The sample was held for 2 h at each step to ensure any size change of the pillars accompanying each step was complete.

Nanopillar *in Situ* and *ex Situ* Imaging. AFM imaging was conducted in both tapping and contact modes by an Agilent 5500 AFM using either Budget SensorsTap-150 probes or Bruker DNP probes. The imaging rate was ~0.9 Hz, and the resolution was 5.4 nm/pix or better. An Agilent designed electrochemical cell compatible with the 5500 AFM was used for *in situ* testing, and the cycling was controlled by a Solartron (SI 1287) Potentiostat. Gwyddion version 2.3 was used for image analysis, and the heights and volumes were calculated using the flat regions of the Ni current collector as the baseline.

SEM imaging was conducted by a Zeiss Auriga SEM. Moisture sensitive samples were transported from the dry room to the SEM in a sealed container with desiccant and exposed to laboratory air for only a few seconds while the SEM was evacuated to vacuum levels.

Conflict of Interest: The authors declare no competing financial interest.

Acknowledgment. The authors acknowledge Dr. Josh Ratchford for his assistance in fabrication of samples. The authors also gratefully acknowledge insightful discussion with Dr. Jeffrey B. Wolfenstine and Dr. Jeffrey A. Read. The authors are grateful to the Army Research Laboratory for financial support. This research was supported in part by an appointment to the Postgraduate Research Participant Program at the U.S. Army Research Laboratory administered by the Oak Ridge Institute for Science and Education through an interagency agreement between the U.S. Department of Energy and USARL.

Supporting Information Available: Additional Raman spectroscopy data, SEM images, and quantitative AFM data. This material is available free of charge *via* the Internet at http://pubs.acs.org.

REFERENCES AND NOTES

1. Tarascon, J. M.; Armand, M. Issues and Challenges Facing Rechargeable Lithium Batteries. *Nature* **2001**, *414*, 359–367.
2. Whittingham, M. S. History, Evolution, and Future Status of Energy Storage. *Proc. IEEE* **2012**, *100*, 1518–1534.
3. Kasavajjula, U.; Wang, C.; Appleby, A. J. Nano- and Bulk-Silicon-Based Insertion Anodes for Lithium-Ion Secondary Cells. *J. Power Sources* **2007**, *163*, 1003–1039.
4. Iwamura, S.; Nishihara, H.; Kyotani, T. Fast and Reversible Lithium Storage in a Wrinkled Structure Formed from Si Nanoparticles During Lithiation/Delithiation Cycling. *J. Power Sources* **2013**, *222*, 400–409.
5. Beaulieu, L. Y.; Eberman, K. W.; Turner, R. L.; Krause, L. J.; Dahn, J. R. Colossal Reversible Volume Changes in Lithium Alloys. *Electrochem. Solid State Lett.* **2001**, *4*, A137–A140.
6. Hatchard, T. D.; Dahn, J. R. *In Situ* XRD and Electrochemical Study of the Reaction of Lithium with Amorphous Silicon. *J. Electrochem. Soc.* **2004**, *151*, A838–A842.
7. Maranchi, J. P.; Hepp, A. F.; Evans, A. G.; Nuhfer, N. T.; Kumta, P. N. Interfacial Properties of the a-Si/Cu: Active-Inactive Thin-Film Anode System for Lithium-Ion Batteries. *J. Electrochem. Soc.* **2006**, *153*, A1246–A1253.
8. Becker, C. R.; Apperson, S.; Morris, C. J.; Gangopadhyay, S.; Currano, L. J.; Churaman, W. A.; Stoldt, C. R. Galvanic Porous Silicon Composites for High-Velocity Nanoenergetics. *Nano Lett.* **2011**, *11*, 803–807.
9. Becker, C. R.; Currano, L. J.; Churaman, W. A.; Stoldt, C. R. Thermal Analysis of the Exothermic Reaction Between Galvanic Porous Silicon and Sodium Perchlorate. *ACS Appl. Mater. Interfaces* **2010**, *2*, 2998–3003.
10. Szczech, J. R.; Jin, S. Nanostructured Silicon for High Capacity Lithium Battery Anodes. *Energy Environ. Sci.* **2011**, *4*, 56–72.
11. Wu, H.; Chan, G.; Choi, J. W.; Ryu, I.; Yao, Y.; McDowell, M. T.; Lee, S. W.; Jackson, A.; Yang, Y.; Hu, L.; et al. Stable Cycling of Double-Walled Silicon Nanotube Battery Anodes through Solid-Electrolyte Interphase Control. *Nat. Nanotechnol.* **2012**, *7*, 309–314.
12. Nie, M.; Abraham, D. P.; Chen, Y.; Bose, A.; Lucht, B. L. Silicon Solid Electrolyte Interphase (SEI) of Lithium Ion Battery Characterized by Microscopy and Spectroscopy. *J. Phys. Chem. C* **2013**, 13403–13412.
13. Philippe, B.; Dedryvère, R.; Gorgoi, M.; Rensmo, H.; Gonbeau, D.; Edström, K. Role of the $LiPF_6$ Salt for the Long-Term Stability of Silicon Electrodes in Li-Ion Batteries—A Photoelectron Spectroscopy Study. *Chem. Mater.* **2013**, *25*, 394–404.
14. Chan, C. K.; Peng, H.; Liu, G.; McIlwrath, K.; Zhang, X. F.; Huggins, R. A.; Cui, Y. High-Performance Lithium Battery Anodes Using Silicon Nanowires. *Nat. Nanotechnol.* **2008**, *3*, 31–35.
15. McDowell, M. T.; Lee, S. W.; Harris, J. T.; Korgel, B. A.; Wang, C.; Nix, W. D.; Cui, Y. *In Situ* TEM of Two-Phase Lithiation of Amorphous Silicon Nanospheres. *Nano Lett.* **2013**, *13*, 758–764.
16. Lee, S. W.; McDowell, M. T.; Berla, L. A.; Nix, W. D.; Cui, Y. Fracture of Crystalline Silicon Nanopillars During Electrochemical Lithium Insertion. *Proc. Natl. Acad. Sci. U. S. A.* **2012**, *109*, 4080–4085.
17. Liu, X. H.; Zheng, H.; Zhong, L.; Huang, S.; Karki, K.; Zhang, L. Q.; Liu, Y.; Kushima, A.; Liang, W. T.; Wang, J. W.; et al. Anisotropic Swelling and Fracture of Silicon Nanowires During Lithiation. *Nano Lett.* **2011**, *11*, 3312–3318.
18. McDowell, M. T.; Ryu, I.; Lee, S. W.; Wang, C.; Nix, W. D.; Cui, Y. Studying the Kinetics of Crystalline Silicon Nanoparticle Lithiation with *In Situ* Transmission Electron Microscopy. *Adv. Mater.* **2012**, *24*, 6034–6041.

19. Liu, X. H.; Fan, F.; Yang, H.; Zhang, S.; Huang, J. Y.; Zhu, T. Self-Limiting Lithiation in Silicon Nanowires. *ACS Nano* **2013**, *7*, 1495–1503.
20. Wu, H.; Cui, Y. Designing Nanostructured Si Anodes for High Energy Lithium Ion Batteries. *Nano Today* **2012**, *7*, 414–429.
21. Li, J.; Dahn, J. R. An *In Situ* X-ray Diffraction Study of the Reaction of Li with Crystalline Si. *J. Electrochem. Soc.* **2007**, *154*, A156–A161.
22. Wang, C.-M.; Li, X.; Wang, Z.; Xu, W.; Liu, J.; Gao, F.; Kovarik, L.; Zhang, J.-G.; Howe, J.; Burton, D. J.; et al. *In Situ* TEM Investigation of Congruent Phase Transition and Structural Evolution of Nanostructured Silicon/Carbon Anode for Lithium Ion Batteries. *Nano Lett.* **2012**, *12*, 1624–1632.
23. Liu, X. H.; Huang, J. Y. *In Situ* TEM Electrochemistry of Anode Materials in Lithium Ion Batteries. *Energy Environ. Sci.* **2011**, *4*, 3844–3860.
24. Huang, J. Y.; Zhong, L.; Wang, C. M.; Sullivan, J. P.; Xu, W.; Zhang, L. Q.; Mao, S. X.; Hudak, N. S.; Liu, X. H.; Subramanian, A.; et al. *In Situ* Observation of the Electrochemical Lithiation of a Single SnO_2 Nanowire Electrode. *Science* **2010**, *330*, 1515–1520.
25. Liu, X. H.; Liu, Y.; Kushima, A.; Zhang, S.; Zhu, T.; Li, J.; Huang, J. Y. *In Situ* TEM Experiments of Electrochemical Lithiation and Delithiation of Individual Nanostructures. *Adv. Energy Mater.* **2012**, *2*, 722–741.
26. Lee, S. W.; McDowell, M. T.; Choi, J. W.; Cui, Y. Anomalous Shape Changes of Silicon Nanopillars by Electrochemical Lithiation. *Nano Lett.* **2011**, *11*, 3034–3039.
27. He, Y.; Yu, X.; Li, G.; Wang, R.; Li, H.; Wang, Y.; Gao, H.; Huang, X. Shape Evolution of Patterned Amorphous and Polycrystalline Silicon Microarray Thin Film Electrodes Caused by Lithium Insertion and Extraction. *J. Power Sources* **2012**, *216*, 131–138.
28. Beaulieu, L. Y.; Hatchard, T. D.; Bonakdarpour, A.; Fleischauer, M. D.; Dahn, J. R. Reaction of Li with Alloy Thin Films Studied by *In Situ* AFM. *J. Electrochem. Soc.* **2003**, *150*, A1457–A1464.
29. Mogi, R.; Inaba, M.; Iriyama, Y.; Abe, T.; Ogumi, Z. Surface Film Formation on Nickel Electrodes in a Propylene Carbonate Solution at Elevated Temperatures. *J. Power Sources* **2002**, *108*, 163–173.
30. Mogi, R.; Inaba, M.; Jeong, S. K.; Iriyama, Y.; Abe, T.; Ogumi, Z. Effects of Some Organic Additives on Lithium Deposition in Propylene Carbonate. *J. Electrochem. Soc.* **2002**, *149*, A1578–A1583.
31. Hertzberg, B.; Benson, J.; Yushin, G. *Ex Situ* Depth-Sensing Indentation Measurements of Electrochemically Produced Si-Li Alloy Films. *Electrochem. Commun.* **2011**, *13*, 818–821.
32. Pharr, M.; Zhao, K.; Wang, X.; Suo, Z.; Vlassak, J. J. Kinetics of Initial Lithiation of Crystalline Silicon Electrodes of Lithium-Ion Batteries. *Nano Lett.* **2012**, *12*, 5039–5047.
33. Sethuraman, V. A.; Srinivasan, V.; Bower, A. F.; Guduru, P. R. *In Situ* Measurements of Stress-Potential Coupling in Lithiated Silicon. *J. Electrochem. Soc.* **2010**, *157*, A1253–A1261.
34. Sethuraman, V. A.; Chon, M. J.; Shimshak, M.; Srinivasan, V.; Guduru, P. R. *In Situ* Measurements of Stress Evolution in Silicon Thin Films During Electrochemical Lithiation and Delithiation. *J. Power Sources* **2010**, *195*, 5062–5066.